Observation of Night OH in the Mesosphere

H. M. Pickett and W. G. Read

Jet Propulsion Laboratory, Calif. Inst. of Tech., Pasadena, California, USA

K. K. Lee and Y. L. Yung

Div. Geological and Planetary Sciences, Calif. Inst. of Tech., Pasadena, California, USA

Satellite measurements from the Aura MLS instrument show a layer of OH near 82 km in the night. This layer confirms earlier measurements by ground-based LIDAR. The MLS and LIDAR observations measure OH in the lowest vibrational state and are distinct from vibrationally-excited emission from the OH Meinel bands in the near infrared. The Caltech 1-D model has been extended to include vibrational dependence of OH reactions and shows good agreement with MLS OH data and with observations of the Meinel bands. The model shows a chemical lifetime of HO_x that increases from less than a day at 80 km to over a month at 87 km. Above this altitude transport processes become an important part of HO_x chemistry. The model prdicts that ground state OH represents 99% of the total OH up to 84 km.

1. Introduction

The Aura satellite was launched on July 15, 2004 into a sun-synchronous near-polar orbit. The Microwave Limb Sounder (MLS) instrument on the Aura satellite has the capability to measure OH in both day and night [*Waters et al., 2006*] using thermal emission from 2.5 THz rotational lines in the ground vibrational state. Further details on the THz module and the OH measurement and calibration are given in *Pickett*[*2006b*]. Validation of MLS stratospheric OH and HO_2 using balloon-based remote sensing are given in *Pickett et al.* [*2006a*]. MLS observations of OH taken in a 24.6 s limb scan extend over 18–94 km, although measurements below 35 km require averaging of multiple scans. The spatial sampling near the equator is 1.5° in latitude and 22.5° in longitude. The local solar time (LST) at the equator is 13.8 hr and 1.8 hr for the ascending and descending parts of the orbit, respectively. The LST is the same for each orbit at a given latitude. At the northernmost latitude (81.8N) LST = 7.8 hr, and at the southernmost latitude (81.8S) LST = 19.8 hr. However, between 70S and 70N the LST only changes by 1.6 hr from the equatorial values.

With version 1.51 of the MLS production retrieval software, we have consistently observed a layer of OH near 82 km on the night portion of the orbit. Unfortunately, the retrieved OH from this version of this production software is is not recommended above 60 km, due to systematic errors that are understood and will be corrected in v2.0 of the software due to be released in 9/2006. Even with these improvements, the retrievals still assume a profile that is piecewise-linear in log pressure with a 6 per decade sampling interval. The special retrievals presented in this paper assume that there is a single layer with a fitted height, width, and OH column.

A night layer in mesospheric OH near 82 km was observed previously with ground-based LIDAR measurements from Table Mountain in Wrightwood, CA [*Brinksma et al., 1998a and 1998b*]. The LIDAR measurements detect resonant fluorescence of OH in the UV and are sensitive to OH in the ground vibrational state. In contrast, OH airglow measurements in the near infrared are due to emission from vibrationally excited OH generated by reaction of atomic H with O_3. Satellite measurements of Meinel band night-glow has shown that the vibrationally excited OH has a peak altitude of 87 km [*Zhang and Shepherd, 1999*]. The peak emission altitude is inversely correlated with the strength of the emission [*Yee et al, 1997*] and also has a seasonal dependence [*Liu and Shepherd, 2006*]

2. MLS Observations

The first step in use of MLS emission is to calibrate the data using a procedure that is a slight modification from the calibration described in *Pickett*[*2006b*]. The first change is that the gain is now assumed to have a sin, cosine dependence on orbital phase as well as a constant dependence assumed previously. This change is needed to account for small thermal effects on gain observed in the satellite data. The second change is that the radiometric zero is derived only from the space view, while before it was derived from both the space view and the calibration target. This change makes small radiances less sensitive to assumptions about the gain with some loss in precision relative to v1.51. Both changes will be part of v2.0 level 1 processing.

The second step is to take a difference the center OH channel and the average of the adjacent channels that are separated by 6 MHz. The MLS OH line profile is in the Doppler limit for altitudes above the 1 hPa level. Since the Doppler width of the MLS OH lines is ∼6 MHz, the radiance difference (ΔR) is sensitive to mesospheric OH while discriminating against baseline and continuum effects. ΔR is still a function of limb observation angle and all data for tangent heights above 1 hPa are used.

The model ΔR comes from a simulated forward model calculation for a triangular layer of OH that has a width of 1/6 decade in pressure (∼2.6 km) and located at 0.00681 hPa. The forward model includes field-of-view and frequency smearing and is corrected for the temperature of the layer. Wider layers are synthesized by shifting the radiance from the triangular layer by a multiple of 1/6 decade spacing and summing to give the radiance expected for a trapezoidal-shaped layer. This layer can have arbitrary center but discrete widths. The calculated ΔR vs scan angle can then be interpolated to experimental scan angles. The temperature of the layer and mapping of scan angle and tangent height into tangent pressure uses retrieved temperature and geopotential height vs. pressure obtained from v1.51 products for the same scan time. This simplified simulation

0094-8276/06/$5.00

approach works because the radiance responds linearly to OH concentration and because the limb sounding geometry does not depart substantially from the reference case.

Figure 1 shows the fitted mean height of the OH night profiles as a function of latitude for Sept. 23, 2004 for solar zenith angles (SZA) $> 100^\circ$. This limit assures that no sunlight illuminates the sampled atmosphere below 100 km. The precision in the fitted height is ∼1 km. Figure 2 shows the fitted column of OH for the same day as Figure 1. The precision in the fitted column is 10%. In both figures, the fitted widths are designated with different colors. The model results to be discussed below are located at the intersection of the two red lines. Note that the fitted column is not correlated with the width, indicating that variability in width conserves the amount of OH.

Figure 3 shows the zonal mean of fitted night OH for June 22, 2005, a date chosen to maximize the hemispheric differences. The vertical white line near 76S latitude indicates the latitude below which the SZA is $> 100^\circ$ throughout the day. The distribution of the night OH seems unaffected by the absence of sunlight. The black line indicates the height of the 0.01 hPa pressure surface. Its slope is due to the fact that the mesospheric temperature is 100 K colder in the summer pole than in the winter pole. Clearly, pressure is a better coordinate for the night OH layer than is altitude.

3. Model Predictions

A simplified version of the one dimensional Caltech/JPL photochemical model is used in this study. Detailed descriptions of the model are given in *Allen et al.* [*1981*]. In the current work, the model involves H, O, and N atoms, 25 species, and 155 reactions, with updates of kinetics rate coefficients from *Sander et al.* [*2002*]. Photodissociation rates are evaluated on-line at each time step, although the effect of scattering has not been taken into account. The model atmosphere consists of 89 vertical layers from 0 to 130 km with vertical resolution of 2 km from 0 to 74 km, 90 to 130 km, and a higher resolution of 0.5 km from 75 to 90 km for the night OH peak. The profiles of temperature and eddy diffusion coefficient, solar flux spectrum are originally taken from *Allen et al.* [*1981*]. The solar irradiance in the Lyman-alpha region near 121.6 nm is increased by 24% to 2.969×10^{11} photons/cm^{2}s in order to correct the variations in the 11 year solar cycle.

An important change is to treat the vibrationally excited states of OH for $v = 0 \ldots 9$ as separate chemical species. The primary source of excitation is the reaction $H + O_3$ [*Nelson et al., 1990*]. Quenching of OH vibrational excitation occurs by spontaneous emission in the Meinel bands as well as by collisional relaxation. The model uses recommendations of *Adler-Golden*, [*1997*] for both quenching mechanisms.(see auxiliary material[1])

The model predictions shown in Figures 1,2 show excellent agreement with measurement. Figure 4 shows a comparison with the LIDAR measurements. Both show a layer at 81 km that is only 1.6 km wide. The model shows less variation of amplitude with time than do the LIDAR measurements. The peak absolute concentration derived from LIDAR is 21 times smaller than the model, but calibration of the absolute value of the return signal is very difficult.

Satellite measurements of this band shows that the OH emission from the (8–3) Meinel band has a peak altitude of 87–89 km and a width of 10 km [*Zhang and Shepherd, 1999, Yee et al, 1997, and Liu and Shepherd, 2006*]. Figure 5 shows the predicted profile of this band for 3 values of LST. These predictions are in general agreement with the satellite observation as well as previous calculations of *Adler-Golden*, [*1997*].

A key property of hydrogen chemistry is the chemical lifetime since it sets the timescale for influence of dynamics. If we define the HO_x density to be $[HO_x] = [OH] + [HO_2] + [H]$, then the HO_x lifetime is $[HO_x]$ divided by the loss rate of HO_x. Below 60 km the lifetime is less than 600 s and [OH] can be calculated using photochemical equilibrium [*Pickett and Peterson, 1996*]. Figure 6 shows the chemical lifetime at higher altitudes. The striking feature is that lifetime varies dramatically with height. By 85 km (0.0042 hPa) the lifetime is 30 days. The explanation for the behavior in Figure 3 near the south pole is that (1) HO_x (principally H) is generated at sunlit latitudes, (2) is transported poleward above 85 km, and (3) descends to 80 km where H reacts with O_3 at night.

With the importance of vibrationally excited OH established for the studies of airglow, it is reasonable to inquire whether MLS measurements of OH need to be corrected for presence of vibrationally excited OH. Figure 6 shows the concentrations of OH as a function of vibration. From this it is clear that the correction to night OH below 84 km (0.005 hPa) is <1% rising to 20% at 90 km (0.002 hPa). In the day vibrationally excited OH is much lower because O_3 is photo-dissociated. On the other hand, ground state OH is present in significant amounts below 80 km because of other reactions that compete with H + O_3.

The model also provides insight into the cause of the narrow OH night layer. In the stratosphere and lower mesosphere, [H] is a minor fraction of $[HO_x]$ and >95% of H combines with O_2 to form HO_2 rather than reacting with O_3. In the region of 80–85 km, three-body formation of HO_2 becomes less important because the rate depends on square of the total pressure. This increases the [H] fraction and increases the importance of the H + O_3 reaction. At slightly higher altitudes, [O] starts increasing rapidly with height because three-body formation of O_3 from O also depends on the square of pressure. The increase in [O] suppresses both [OH] and $[HO_2]$ through the reactions with O. The lifetime of HO_x increases with height because the loss depends on [OH] and $[HO_2]$, but not directly on [H].

4. Conclusions

Observations from Aura MLS of OH in its ground vibrational state show a night layer at 82 km, confirming earlier ground-based LIDAR measurements. A modified version of the Caltech 1-D model predicts a very narrow 1.6 km wide layer that is consistent with the LIDAR. However, MLS retrievals show a distribution of widths from 1.6 km to 10.8 km with a global mean of 8.3 km that is most likely due to transport. The model does not include transport (other than vertical eddy diffusion). The LIDAR measurements are a limited sample and the technique is less sensitive to broad layers.

The layer observed by MLS is distinct from Meinel-band night-glow emission from vibrationally excited OH. However, examination of the model calculations show that both originate from the H + O_3 reaction. The difference in the altitude of the two layers is due to the effect of pressure on collisional quenching of the vibrational excitation. The Meinel emission is inhibited by collisional quenching while both the emission and quenching favor observation of ground state OH.

The pressure level of 0.0042 hPa (85 km) is a critical pressure for OH. For altitudes below this pressure, more than 99% of the OH is in the ground vibrational state and chemistry is local. For altitudes above this pressure, there is an increasing fraction of OH in excited states and the chemical lifetime is longer than a month. Therefore, modeling of OH at altitudes above this critical pressure requires explicit description of long-term transport as well as explicit inclusion of OH vibrational state dependent chemistry.

Acknowledgments. We wish to thank all who helped make the Aura OH measurements possible. KKL was supported by a Summer Undergraduate Research Fellowship at the California Institute of Technology. YLY was supported by NASA grant NNG04GD76G to the California Institute of Technology. Research at the Jet Propulsion Laboratory, California Institute of Technology, is performed under contract with the National Aeronautics and Space Administration.

Notes

1. Auxiliary material is available at ftp://ftp.agu.org/apend/gl/2006GLXXXXXX.

References

Adler-Golden, S., Kinetic Parameters for OH Nightglow Modeling Consistent with Recent Laboratory Measurements, *J. Geophys. Research, 102*, 19969-19976, 1997.

Allen, M., Y. L. Yung, and J. W. Waters, Vertical Transport and Photochemistry in the Terrestrial Mesosphere and Lower Thermosphere (50-120 km), *J. Geophys. Research, 86*, 3617-3627, 1981.

Brinksma, E. J., et al., First Lidar Observations of Mesospheric Hydroxyl, *Geophys. Res. Lett., 25*, 51-54, 1998.

Brinksma, E. J., et al., Correction: First Lidar Observations of Mesospheric Hydroxyl, *Geophys. Res. Lett., 25*, 521, 1998.

Liu, G., and G. G. Shepherd, An empirical model for the altitude of the OH nightglow emission, *Geophys. Res. Lett., 33*, L09805, 2006.

Pickett, H. M., et al., Validation of Aura MLS HOx Measurements with Remote-Sensing Balloon Instruments, *Geophys. Res. Lett., 33*, L01808, 2006.

Pickett, H. M., Microwave Limb Sounder THz Module on Aura, *IEEE Trans. Geosci. Remote Sensing, 44*, 1122-1130, 2006.

Pickett, H. M., and D. B. Peterson, Comparison of Measured Stratospheric OH with Prediction, *J. Geophys. Research, 101*, 16789-16796, 1996.

Sander, S. P., *et al.*, Chemical Kinetics and Photochemical Data for Use in Atmospheric Studies: Evaluation 14, *JPL Publication 02-25*, 2002.

Waters, J. W., *et al.*, The Earth Observing System Microwave Limb Sounder (EOS MLS) on the Aura Satellite, *IEEE Trans. Geosci. Remote Sensing, 44*, 1075-1092 (2006).

Yee, J. H., G. Crowley, R. G. Roble, W. B. Skinner, M. D. Burrge, and P. B. Hays, Globaa simulations ans observations of $O(^1S)$, $O_2(^1\Sigma)$ and OH mesospheric nightglow emissions, *J. Geophys. REs., 102*(A9), 19,949-19,968, 1997.

Zhang, S. P., and G. S. Shepherd, The Influence of the Diurnal Tide on the O(1S) and OH Emission Rates Observed by WINDII on UARS, *Geophys. Res. Lett., 26*, 529-532, 1999.

H. M. Pickett and W. G. Read, Jet Propulsion Laboratory, 4800 Oak Grove Drive, Pasadena, CA 91109, USA. (herbert.m.pickett@jpl.nasa.gov)

K . K. Lee and Y. L. Yung, Div. Geological and Planetary Sciences, Calif. Inst. of Tech., Pasadena, California, USA

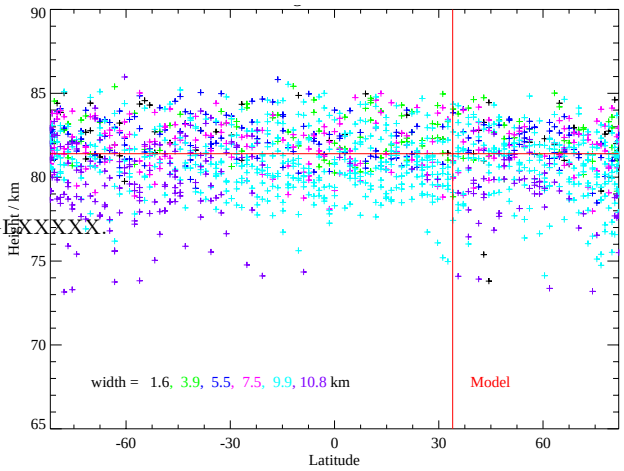

Figure 1. Distribution of the height of the night OH layer on Sept. 23, 2004. Each point represents a single MLS limb scan and its color indicates the measured width.

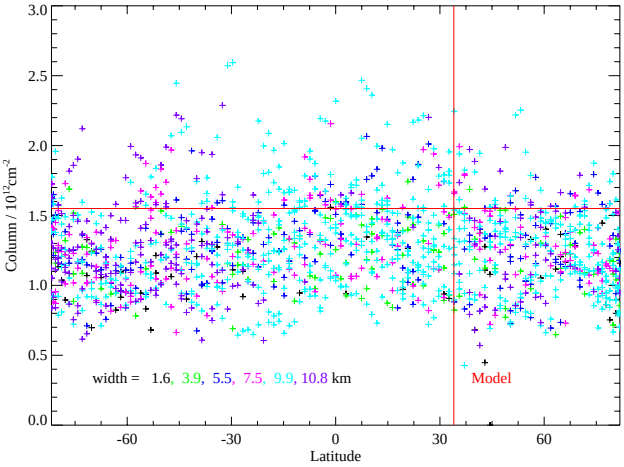

Figure 2. Distribution of the column of the night OH layer. See Figure 1.

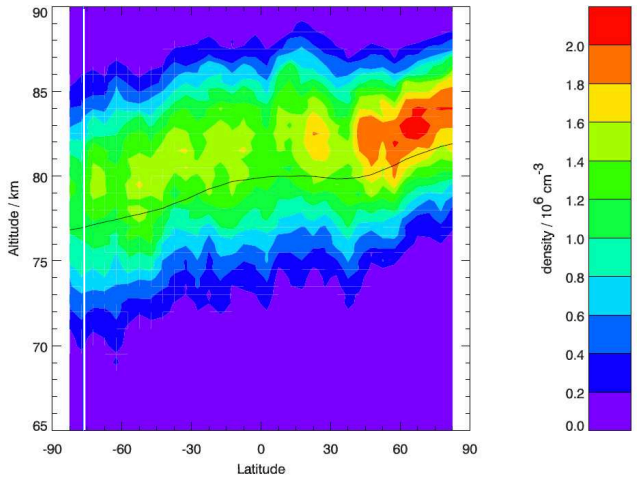

Figure 3. Zonal Mean MLS observations of OH density with SZA of $> 100^\circ$ on June 22, 2005. The black line is the height of the 0.01 hPa pressure level. The vertical white line is the latitude where the noon SZA $= 100^\circ$

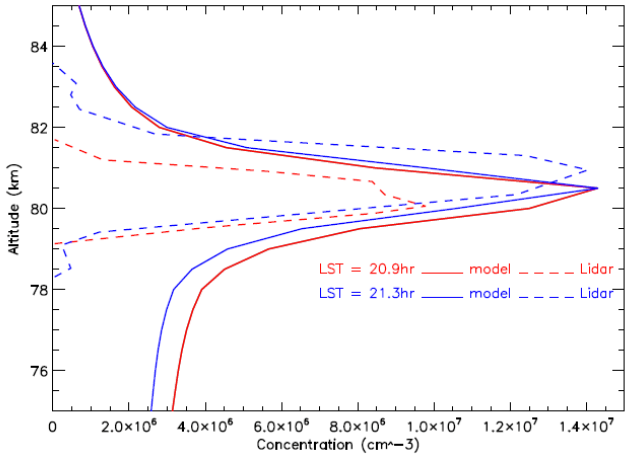

Figure 4. Comparison between model results (solid lines) and LIDAR measurements (dotted lines) for July 17, 1996 at latitude 34N, LST time 20.9hr (red), 21.3hr (blue). Experimental densities are multiplied by 21.

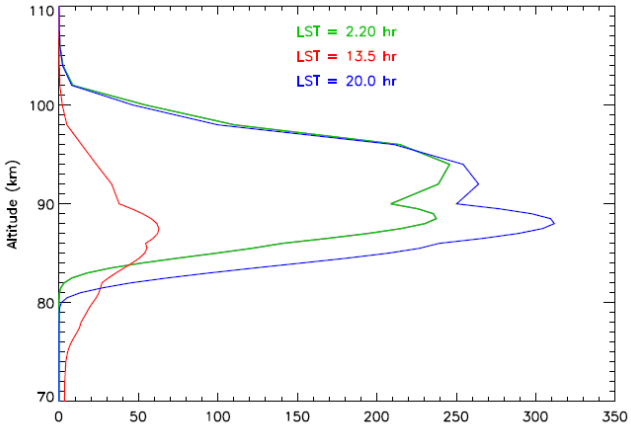

Figure 5. Calculated profiles of the (8-3) band emission rate in photons/cm^{3}s for Sept. 23, 2004 at latitude 34N, LST 2.20hr (green), 13.5hr (red) and 20.0hr (blue).

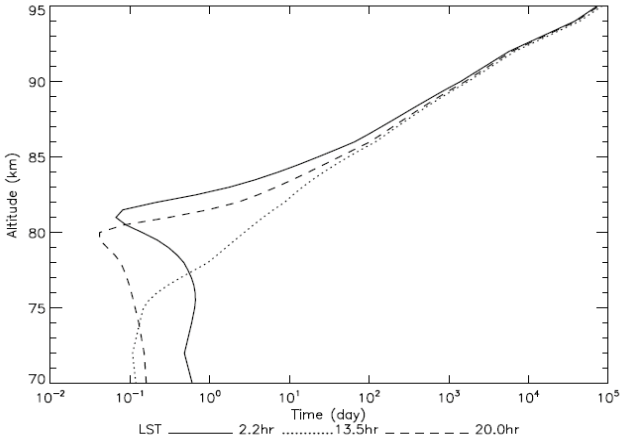

Figure 6. Calculated chemical lifetime of HOx for Sept. 23, 2004 at latitude 34N.

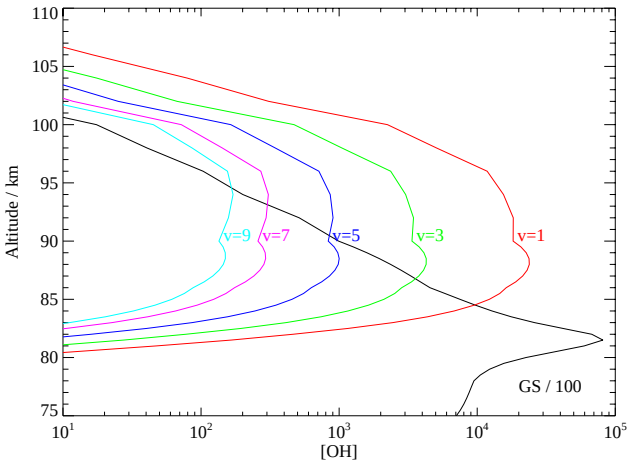

Figure 7. Calculated night profiles of vibrationally excited OH densities for September 23, 2004 at latitude 34N, LST 2.20hr.